JOURNAL OF SOLID STATE CHEMISTRY 81, 9–20 (1989)

Crystal Structure Determination and Rietveld Refinement of $Zn(OH)(NO_3) \cdot H_2O$

L. ERIKSSON

Department of Structural Chemistry, Arrhenius Laboratory, University of Stockholm, S-106 91 Stockholm, Sweden

D. LOUËR

Laboratoire de Cristallochimie (LA 254), Université de Rennes, Avenue du Général Leclerc, F-35042 Rennes Cedex, France

AND P.-E. WERNER

Department of Structural Chemistry, Arrhenius Laboratory, University of Stockholm, S-106 91 Stockholm, Sweden

Received December 19, 1988

The crystal structure of $Zn(OH)(NO_3) \cdot H_2O$ has been studied by X-ray diffraction methods using fibrous microcrystals and powder. The cell dimensions are $a = 17.951$ Å, $b = 3.2600$ Å, $c = 14.272$ Å, and $\beta = 114.91°$. The space group is $P2_1/c$. The structure has been refined by the Rietveld full-profile technique. The results obtained from different data sets and the corresponding discrepancy indicators are compared. The structural chemistry of the compound is discussed and an interpretation of its topotactic transformation into $Zn_3(OH)_4(NO_3)_2$ is presented. © 1989 Academic Press, Inc.

Introduction

Four zinc hydroxide nitrates have been reported: the crystal structures of two of them $Zn_5(OH)_8(NO_3)_2 \cdot 2H_2O$ (*1*) and $Zn_3(OH)_4(NO_3)_2$ (*2*) were solved in single crystal studies. They are characterized by layer structures which are related to the brucite type, and they belong respectively to types IIa and I of the structural classification scheme proposed for the bivalent metal hydroxide nitrates (*3*). Among investigations of their properties, topotactic studies by ion exchange have been described (*4*), as have studies of their role as precursors in the synthesis of zinc oxide with high surface area. This oxide exhibits coherently diffracting domains whose size and shape are amenable to a precise analysis by means of diffraction line broadening (see, for example Ref. (*5*)). The hydroxide nitrate $Zn_5(OH)_8(NO_3)_2$ is obtained by thermal decomposition of the hydrated phase; a possible crystal structure has been proposed from analogies between the unit cell parameters of the two phases (*6*). This suggested layer structure would correspond to type IIb of the structural classification. The fourth known hydroxide nitrate $Zn(OH)(NO_3) \cdot H_2O$ with a lower hydoxyl ion con-

0022-4596/89 $3.00
Copyright © 1988 by Academic Press, Inc.
All rights of reproduction in any form reserved.

tent has a fibrous texture which has precluded a precise structural analysis (*7*). Although the thermal decomposition mechanism of this solid, like that of the layered $Zn_3(OH)_4(NO_3)_2$ compound, involves the formation of gaseous nitric acid and water by a chemical reaction occurring inside the crystallites (*8*), the fibrous texture of the crystals does not seem to be consistent with a layer structure. To clarify this discrepancy, an investigation of the crystal structure is strongly needed.

Recent applications of X-ray powder diffraction, especially in structure analyses utilizing the powerful Rietveld method (see, for example, Refs. (*9, 10*) have further motivated us to investigate the structure of this zinc hydroxide nitrate, $Zn(OH)(NO_3) \cdot H_2O$. Data obtained by four different experimental techniques have been used for the solution and refinement of the crystal structure. The present paper deals with the crystal structure determination of $Zn(OH)(NO_3) \cdot H_2O$, contains a discussion of the results obtained from different sets of data, and, finally, describes the structural chemistry of this solid.

Experimental

Crystals of $Zn(OH)(NO_3) \cdot H_2O$ displaying a fibrous texture were grown, under atmospheric conditions, by slow hydrolysis at 65°C of melted zinc nitrate hexahydrate (*11*). For this work, four types of X-ray diffraction data were collected from the sample.

A small group of fibrous microcrystals of relatively parallel orientation were mounted on a STOE single crystal diffractometer. A total of 607 independent reflections with $I(\text{net}) > 3\sigma(I)$ were collected with θ–2θ scans, using Cu$K\alpha$ radiation and a wide detector opening (4 mm). Attempts to use ω-scans failed because the peaks were too broad in this scan direction. As the data quality was necessarily low, we decided also to use Guinier powder diffraction data and to employ the Rietveld refinement technique to analyze the structure. For the final refinements powder diffractometer data were used.

TABLE I

CRYSTAL DATA FOR $Zn(OH)(NO_3) \cdot H_2O$

Data type	Radiation	Data range	Number of F	R_F	R_{wp}
"Multiple crystal"	Cu$K\alpha$	$(h0l)$	132	0.144	
"Multiple crystal"	Cu$K\alpha$	(hkl)	607	0.241	
Guinier	Cu$K\alpha_1$	$10° < 2\theta < 80°$	456	0.183	0.42
Guinier	Cr$K\alpha_1$	$10° < 2\theta < 85°$	151	0.138	0.41
Siemens	Cu$K\alpha_1$	$10° < 2\theta < 64.5°$	244	0.071	0.18

Note. a = 17.951(3) Å, b = 3.2600(2) Å, c = 14.272(2) Å, β = 114.91°(1), V = 757.5 Å^3, M_{20} = 26, F_{30} = 43(0.010,69), F_{53} = 28(0.010,200).

X-ray diffraction photographs were obtained in a subtraction-geometry Guinier–Hägg camera, 100 mm in diameter, using strictly monochromatized Cu$K\alpha_1$ (λ = 1.5405981 Å) and Cr$K\alpha_1$ (λ = 2.28962 Å) radiation. Single-coated film (CEA, Reflex 15) was used in order to avoid superposition of front- and back-layer intensity profiles and to reduce the background. All the films were measured with a computer-controlled single-beam microdensitometer, LS-18, designed for X-ray powder diffraction photographs (*12*). The dimensions of the slit opening of the collimator were 0.040 × 2.0 mm and the corresponding measuring step length in the θ-direction on the photographs was about 0.0228° (2θ). The θ-scale was calibrated by means of the internal standard technique, using a parabolic correction curve. Silicon (a = 5.430880(35) Å at 25°C) was chosen as the standard substance (*13*). Unit-cell dimensions obtained from least-squares refinement of the Cu$K\alpha_1$ data set are given in Table I. The corresponding indexed powder diagram is given in Table II.

Powder diffractometer data were collected with a Siemens D500 powder diffraction system. Strictly monochromatic Cu$K\alpha_1$ radiation was selected by means of

TABLE II

OBSERVED AND CALCULATED 2θ VALUES FOR THE GUINIER POWDER DIFFRACTION PATTERN OF $Zn(OH)(NO_3) \cdot H_2O$

(hkl)	$2\theta_{obs}$	$\Delta(2\theta)$	d_{obs}	I/I_0
(200)	10.863	0.004	8.138	541
(20̄2)	13.424	0.014	6.591	669
(002)	13.678	0.008	6.469	391
(3̄02)	16.305	0.012	5.432	348
(300)		−0.015		
(102)	16.732	0.009	5.294	225
(40̄2)	20.282	−0.001	4.375	116
(202)	20.807	0.001	4.266	101
(400)	21.819	0.001	4.070	139
(20̄4)	24.958	0.015	3.5649	594
(302)	25.453	0.003	3.4967	111
(10̄4)	25.678	−0.008	3.4664	40
(40̄4)	26.993	−0.014	3.3005	40
(004)	27.531	−0.011	3.2372	40
(110)	27.901	0.002	3.1952	272
(1̄11)		0.036		
(011)	28.210	0.004	3.1608	231
(50̄4)	29.574	−0.010	3.0181	210
(104)	30.347	0.029	2.9429	142
(402)	30.478	0.031	2.9306	90
(21̄2)	30.582	0.019	2.9209	228
(211)	31.351	−0.015	2.8510	273
(3̄12)		0.017		
(310)	32.003	0.003	2.7944	1000
(60̄4)	32.934	0.007	2.7175	40
(1̄13)	33.413	−0.039	2.6796	40
(204)	33.811	−0.005	2.6490	87
(311)		0.033		
(41̄2)	34.269	−0.008	2.6146	215
(70̄4)	36.857	0.000	2.4368	204
(5̄12)	37.296	0.000	2.4091	388
(3̄14)		0.025		
(312)	37.685	−0.012	2.3850	88
(1̄14)		0.009		
(304)	37.869	0.004	2.3739	244
(510)	39.061	−0.006	2.3042	294
(5̄14)	40.721	0.006	2.2140	238
(6̄12)	40.901	−0.007	2.2046	83
(80̄4)		0.034		
(114)	41.274	0.000	2.1856	241
(404)	42.332	−0.008	2.1334	106
(6̄14)	43.308	0.002	2.0875	77
(70̄6)	43.534	−0.006	2.0772	330
(800)	44.488	0.007	2.0349	160
(106)	44.600	0.006	2.0300	293
(7̄14)	46.498	0.007	1.9515	128
(41̄6)	47.505	0.005	1.9124	151
(21̄6)	47.761	0.013	1.9028	163
(8̄14)	50.147	−0.039	1.8177	121
(414)	51.124	−0.010	1.7852	78
(70̄8)	53.630	−0.000	1.7076	92
(8̄16)	54.913	−0.019	1.6707	70
(7̄17)	56.347	0.014	1.6315	80
(10̄4)		−0.032		
(120)	56.726	0.015	1.6215	453
(008)	56.851	−0.006	1.6182	265
(12̄1)		−0.020		
(021)		−0.038		
(121)	57.507	−0.011	1.6013	138
(220)	57.615	−0.012	1.5986	208
(122)	57.988	−0.005	1.5892	167
(22̄2)		0.019		
(910)	58.278	−0.006	1.5820	201
(90̄8)		−0.011		
(41̄8)	58.978	−0.009	1.5648	145

Note. $\Delta(2\theta) = 2\theta_{obs} - 2\theta_{calc}$; $\lambda = 1.5405981$ Å.

an incident-beam curved-crystal germanium monochromator with asymmetric focusing (short focal distance 124 mm, long focal distance 216 mm). The divergence slits located in the incident beam were selected to ensure complete illumination of the specimen surface at 12° (2θ). With these experimental conditions, the instrumental resolution curve, obtained from a standard material (BaF_2) reaches a minimum full width at half-maximum (FWHM) value (0.065° (2θ)) at about 30° (2θ) which rises to twice that value at about 125° (2θ).

The powder diffraction pattern was scanned in steps of 0.02° (2θ), and fixed-time counting (20 sec) was employed. At the end of the data collection the stability of the intensity of the incident beam was checked by recording the first lines of the pattern. To minimize preferred orientation effects due to the fibrous morphology of the crystallites, the zinc hydroxide nitrate was ground for $\frac{1}{2}$ hr, and a side-loading method was used to prepare the sample for the diffractometer.

Structure Determination

From the systematically absent reflections ($h0l$) with $l = 2n + 1$ and ($0k0$) with $k = 2n + 1$ the space group $P2_1/c$ proposed by Louër *et al.* (*7*) was confirmed. The Zn positions were derived from a three-dimensional Patterson function using the STOE data set. Since the b-axis is as short as 3.26 Å (Table I), we decided to determine the x- and z-coordinates from the ($h0l$) reflections

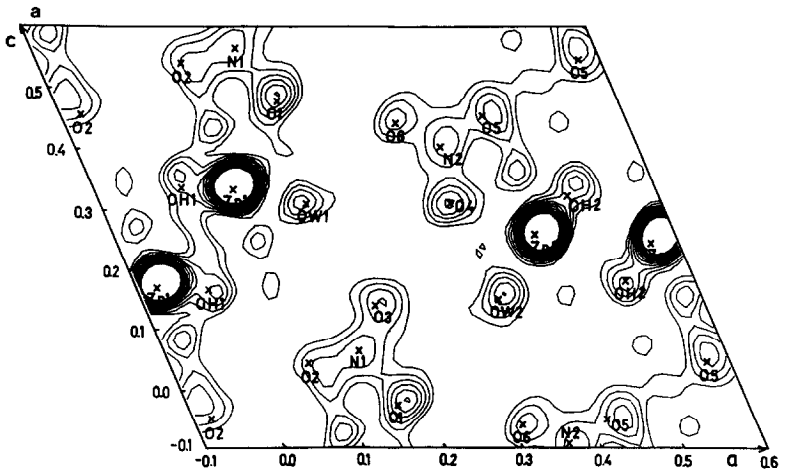

FIG. 1. Electron density projections (x, z) calculated from (a) a STOE data set obtained from a small group of fibrous microcrystals of relatively parallel orientation; (b) a Cr$K\alpha_1$ Guinier powder data set; and (c) a Cr$K\alpha_1$ Guinier powder data set using a definition range of one FWHM in refinements of the zinc atom positions. No other atoms were included in this calculation. For maps (a) and (b) all atomic positions were used. In maps (a), (b), and (c) the final atomic positions as obtained from the Cr$K\alpha_1$ data set are marked.

and to derive the y-coordinates from the general reflections.

Although it was possible to determine all oxygen and nitrogen positions by Fourier methods and to refine them by least-squares calculations to a conventional structure factor R_F-value = 0.144 ($R_F = \Sigma||F|_{obs} - |F|_{calc}|/\Sigma|F|_{obs}$) from the ($h0l$) reflections, two relatively strong extra peaks at (xz) = (0.07, 0.43) and (0.07, 0.25) were obtained in the final electron density projection map (see Fig. 1a). In the corresponding Fourier map, calculated with structure factors from the Cr$K\alpha_1$ Guinier data set by the profile program (*14*), no extra peaks were found (Fig. 1b). The positional parameters were identical within two SDs in the two calculations. The R_F-value obtained for the Cr$K\alpha_1$ Guinier data set was 0.138, although the profile R-values R_p and R_{wp} were 0.40 and 0.41, respectively. The y-coordinates were determined and refined from the three-dimensional STOE data set. Since the final R_F-value was as high as 0.24, we decided to check this result by means of the Cu$K\alpha_1$ Guinier powder data. Using identical positional parameters, the R_F-value obtained for 456 reflections derived by the profile program was 0.183. The profile R-values, however, were $R_p = R_{wp} = 0.42$.

Although it was not necessary to derive the structure completely from the powder data sets, it may be of interest in principle to discuss the possibilities of solving the structure solely from powder diffraction data. Therefore, the zinc atom positions and the profile parameters were refined with the Cr$K\alpha_1$ data set. The Cr data set was chosen in order to minimize the number of overlaps.

The definition range of the profile function for a single profile in the refinements of a complete structure may be set equal to three times the FWHM. As stated by Toraya (*15*) the definition range should be extended for the strong reflections to include

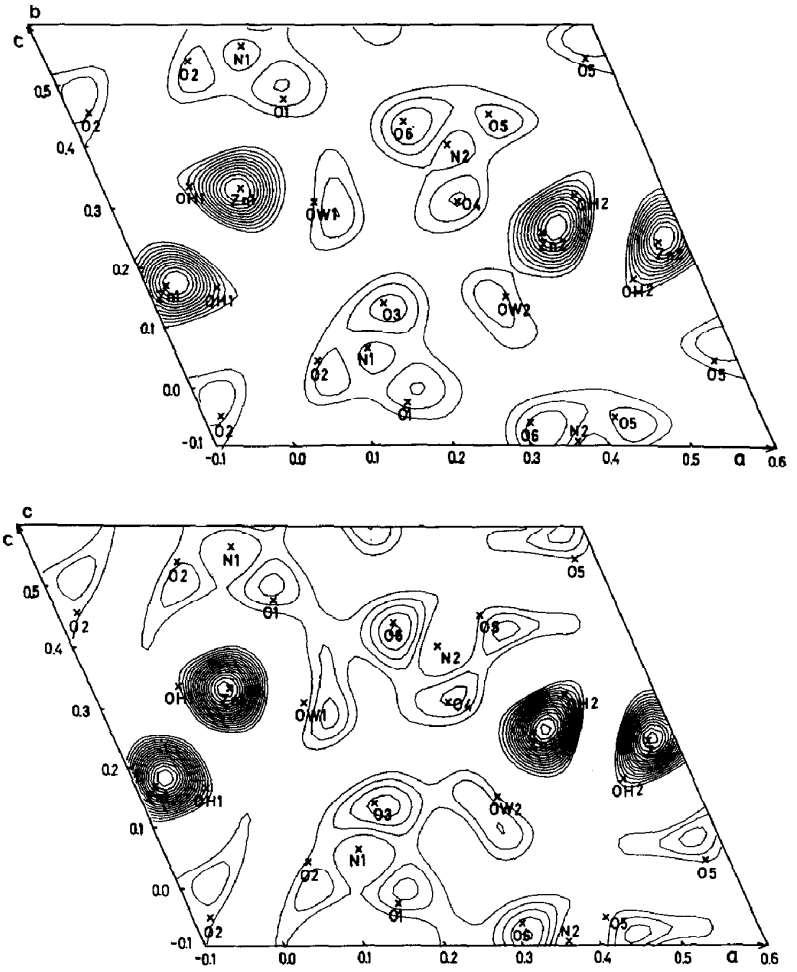

FIG. 1—*Continued*

>99% of the profile area in order to suppress large truncation errors in overlapping weak reflections.

In the preliminary stage of a structure determination, however, when only a small part of the structure is included, it may be preferable to decrease the definition range to one FWHM in order to suppress the influence of erroneous distribution of the observed intensities. This may be regarded as an intermediate step between the uses of peak intensities and integrated profiles. The Fourier map in Fig. 1c was calculated from the Cr data set using only the zinc positions and one FWHM in the profile refinement. Although the deviations of the final atom positions from the Fourier peak positions are sometimes large, the basic structure may be recognized. A corresponding Fourier map using three FWHM in the profile refinements was somewhat less accurate.

A comparison of the observed and calculated Guinier patterns showed a general tendency for the peaks to be higher for the observed than for the calculated intensities.

This is partly compensated by broader profiles in the calculated patterns. This may also explain the large differences between the structure factor R-values and the profile R-values. The R_F-values obtained from the powder data sets and the STOE data are similar, however, and the positional parameters showed no significant differences.

Several runs were also made using fixed half-width parameters determined from observed individual peaks. Although in this way better agreement was found between observed and calculated peak widths, the R-values were never improved and the positional coordinates did not change significantly. Preferred orientation errors may occur, but since this peak width problem has been observed in the output from several profile refinements of Guinier patterns, it may be concluded that the main explanation must be found in a strong θ-dependency of the profile shapes. In the determination of structures from powder diffraction data, the high resolution in Guinier patterns is favorable. For more accurate refinements, powder diffractometer data showing more mathematically well-defined profile function should be preferable.

From the present investigation, as well as from earlier experience with Guinier powder data refinements, however, we conclude that the quality of a structure determination is usually better illustrated by the structure factor R-value, R_F, than by the profile R-values, R_p and R_{wp}. This conclusion is not rigorous and may be violated if the structural constraints are too lenient.

Refinement

Final refinements of the structure were made with the Siemens D500 powder diffractometer data set. The consistency of the previous refinements was checked with the program DBW3.2S (*16*), which is a successor to the program described in Ref. (*17*). A modified Lorentzian function (Mod. 2 Lorentzian) was used for representation of the individual reflection profiles. The angular dependence of the peak FWHM was described by the usual quadratic form in tan (θ)

$$\mathrm{FWHM}^2 = U*\tan^2(\theta) + V*\tan(\theta) + W,$$

where U, V, and W are parameters whose values were refined. The background intensity was evaluated in regions without contribution from Bragg reflections, and linear interpolation of these values led to the background correction. Due to the high density of diffraction lines, the upper limit for background estimation was fixed at 64.5° (2θ). Thus the refinement was carried out using the angular range $12° < 2\theta < 64.5°$. Integral intensities were distributed over three FWHM on either side of a diffraction line profile. The profile analysis refinement involved the following parameters: 42 atomic coordinates, 14 isotropic temperature factors, one scale factor, one zero-point parameter, four cell parameters, one asymmetry parameter, and three half-width parameters. In order to adjust the peak position and the fit between the analytical profile shape and the observed line profiles, the cell and profile parameters were allowed to vary from time to time during the refinement process. The nitrate groups, which are linked to Zn atoms by only one oxygen atom, suffered significant coordinate shifts, leading to unsatisfactory distances and angles. Consequently, a progressive refinement of their coordinates was performed by allowing a maximum variation of 20% in each cycle. The last variable to be refined was the preferred-orientation factor (G1 = 0.15). The final R-values, $R_p = 0.137$, $R_{wp} = 0.184$, $R_B = 0.103$, and $R_F = 0.071$, were obtained for the parameters listed in Table III. Figure 2 shows the fit obtained between the calculated and the observed patterns.

A comparison between the 42 coordi-

nates in Table III and the corresponding coordinates obtained from the Guinier data sets showed that 30 values agreed within one SD, six within two SDs, and six (of which five are y-coordinates) within three SDs. Bond lengths and bond angles as obtained from the final refinement are listed in Table IV.

TABLE III

POSITIONAL AND THERMAL PARAMETERS OF $Zn(OH)(NO_3) \cdot H_2O$

Atom	Site	x	y	z	B (Å^2)
Zn(1)	4(*e*)	0.0716(3)	0.248(2)	0.3281(4)	0.6(2)
Zn(2)	4(*e*)	0.4284(4)	0.376(2)	0.2531(5)	1.7(2)
$O_{aq}(1)$	4(*e*)	0.162(1)	0.828(9)	0.303(2)	0.4(8)
O(1)	4(*e*)	0.168(1)	0.177(8)	−0.021(2)	0.1(8)
O(2)	4(*e*)	0.070(2)	0.293(9)	0.036(2)	0.0(8)
O(3)	4(*e*)	0.191(2)	0.000(7)	0.134(2)	0.2(8)
N(1)	4(*e*)	0.136(2)	0.16(1)	0.048(2)	0.0(8)
OH(1)	4(*e*)	0.001(1)	0.769(9)	0.336(1)	0.7(7)
$O_{aq}(2)$	4(*e*)	0.348(2)	0.966(9)	0.143(2)	4.1(9)
O(4)	4(*e*)	0.335(2)	0.493(9)	0.308(2)	4.4(1.1)
O(5)	4(*e*)	0.424(2)	0.274(10)	0.455(2)	2.3(1.1)
O(6)	4(*e*)	0.335(2)	0.675(11)	0.457(3)	7.0(1.2)
N(2)	4(*e*)	0.362(3)	0.441(16)	0.415(4)	7.4(1.9)
OH(2)	4(*e*)	0.497(1)	0.857(8)	0.330(2)	1.5(8)

Discrepancy Indices

The quantities used to estimate the agreement between the observations and the model during the course of a Rietveld refinement can be written as

The profile R_p

$$= \frac{\sum |y_i(\text{obs}) - (1/c)y_i(\text{calc})|}{\sum y_i(\text{obs})}$$

The weighted profile R_{wp}

$$= \left[\frac{\sum w_i[y_i(\text{obs}) - (1/c)y_i(\text{calc})]^2}{\sum w_i[y_i(\text{obs})]^2}\right]^{1/2}$$

The Bragg $R_B = R_I$

$$= \frac{\sum |I(\text{“obs”}) - I(\text{calc})|}{\sum I(\text{“obs”})}$$

The structure factor R_F

$$= \frac{\sum |I(\text{“obs”})^{1/2} - I(\text{calc})^{1/2}|}{\sum I(\text{“obs”})^{1/2}}$$

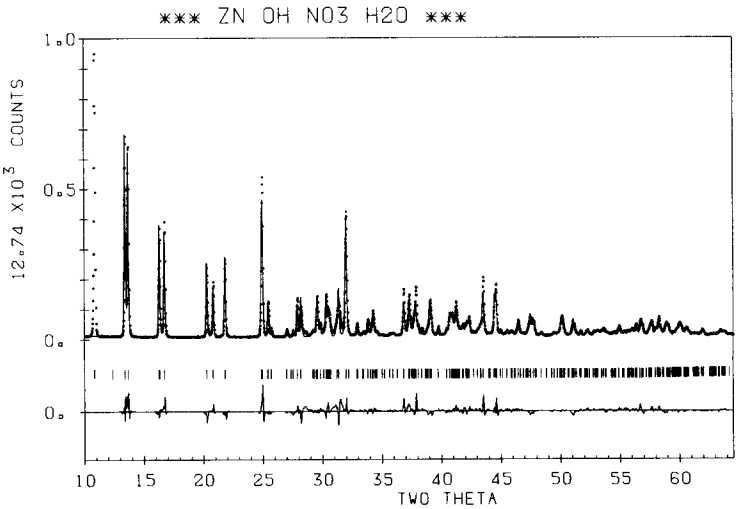

FIG. 2. The final Rietveld difference plot of $Zn(OH)(NO_3) \cdot H_2O$ from the Siemens D500 data set. The upper trace shows the observed data as dots, and the calculated pattern is shown by the solid line. The lower trace is a plot of the difference: observed minus calculated. The vertical markers show positions calculated for Bragg reflections.

TABLE IV

SELECTED INTERATOMIC DISTANCES (Å) AND ANGLES (°), WITH ESTIMATED STANDARD DEVIATIONS IN PARENTHESES

Zn(1)–OH(1)^{i}	2.05(3) Å	Zn(2)–OH(2)	2.01(3) Å
–O(1)^{ii}	2.14(2)	–O$_{aq}$(2)^{i}	2.10(3)
–OH(1)^{iii}	2.15(3)	–OH(2)^{i}	2.11(3)
–OH(1)	2.16(2)	–OH(2)^{iv}	2.13(2)
–O$_{aq}$(1)^{i}	2.27(3)	–O(4)	2.16(3)
–O$_{aq}$(1)	2.62(3)	–Oaq(2)	2.52(3)

OH(1)–Zn(1)–O$_{aq}$(1)^{i}	165(6)°
OH(1)^{i}–Zn(1)–O$_{aq}$(1)	174.9(8)
O(1)^{ii}–Zn(1)–OH(1)^{iii}	163.3(9)
OH(2)–Zn(2)–Oaq(2)^{i}	167(1)°
OH(2)^{i}–Zn(2)–O$_{aq}$(2)	173.2(9)
O(4)–Zn(2)–OH(2)^{iv}	166(1)

N(1)–O(2)	1.22(4) Å	N(2)–O(5)	1.16(6) Å
–O(3)	1.31(4)	–O(6)	1.20(6)
–O(1)	1.33(4)	–O(4)	1.41(5)

O(1)–N(1)–O(2)	125(3)°	O(4)–N(2)–O(5)	112(4)°
O(1)–N(1)–O(3)	109(3)	O(4)–N(2)–O(6)	115(4)
O(2)–N(1)–O(3)	126(3)	O(5)–N(2)–O(6)	127(4)

Possible hydrogen bonds

Oaq(1)–O(3)^{v}	2.73(3) Å	Oaq(2)–O(6)^{vi}	2.60(4) Å
–O(6)	2.99(4)	–O(3)^{v}	2.78(4)

O(3)^{v}–O$_{aq}$(1)–O(6)	99(1)°
O(3)^{v}–O$_{aq}$(2)–O(6)^{vi}	107(1)

Note. Codes: i $(x, y - 1, z)$, ii $(x, \frac{1}{2} - y, z + \frac{1}{2})$, iii $(-x, y - \frac{1}{2}, \frac{1}{2} - z)$, iv $(1 - x, y - \frac{1}{2}, \frac{1}{2} - z)$, v $(x, 1 + y, z)$, vi $(x, \frac{3}{2} - y, z - \frac{1}{2})$.

The expected R_{exp}

$$= R_E = \left[\frac{N - P}{\sum w_i[y_i(\text{obs})]^2}\right]^{1/2}$$

The goodness of fit $GF = \left[\frac{R_{wp}}{R_{exp}}\right]^2$.

The quantity c is a refinable scale factor. The values y_i (obs) and y_i (calc) are the observed and calculated intensities at point i in the pattern. From a statistical point of view they should also contain the background intensities. Because of technical restrictions this is not always possible, however. Intensity data from a Guinier photograph may be obtained from optical densities above the local background and therefore the true background may not be included in the measurement. The background intensity will also affect the weight w_i which is normally set to $1/y_i$ (obs), from counting statistics. In the case of photographic data the lack of background information may be compensated for by using a constant weight for all intensities below a threshold value.

The observed and calculated integrated Bragg intensities are denoted I("obs") and I(calc). The reason for the quotation marks is the fact that the observed intensities are calculated by partitioning the raw data in accordance with the calculated intensities of the component peaks. The number of step intensities and parameters refined are denoted N and P, respectively, in the factors listed above. N is normally the number of step intensities within the integration range of the Bragg reflections. One may argue, however, that if the background is included in the refinement, it should preferentially be refined from areas outside the Bragg reflections.

The quantity minimized in a Rietveld refinement is the weighted profile R-value, R_{wp}. Its numerical value may be somewhat misleading, however (*18*). This is because it is more dependent on the background, the length of the reflection tails, the applied weights, and the profile function than on the integrated intensities. The main question is: How well are the integrated intensities distributed between the reflections when the weighted profile R-value reaches its minimum? There is an obvious risk of obtaining false minima. The risk is reduced, however, if the resolution of the pattern is increased and if the most accurate profile function is used. It should also be noted that the weighted profile R-value cannot be used to compare structure refinements from different types of powder diffraction data.

TABLE V

COMPARISON OF DISCREPANCY INDICES BETWEEN ORIGINAL SIEMENS D500 DATA AND DATA WITH SIMULATED HIGH BACKGROUND

Discrepancy index type	Original data	Simulated data[a]
R_p	0.137	0.026
R_{wp}	0.184	0.038
R_{exp}	0.043	0.020
GF	18.3	3.6
R_B	0.103	0.092
R_F	0.071	0.067

[a] Two thousand added to all step intensities.

Comparisons are possible only by using the Bragg and the structure factor R-values. They can be used to judge not only the quality of the fitted profile but also the quality of the structure determination. The most obvious way to illustrate this statement is to add a high artificial constant background intensity to all step intensities and repeat the refinement. In an experiment a high background may be obtained by using badly monochromatized radiation and therefore the simulated data will correspond to lower quality data.

In the present case the background obtained for the Siemens D500 data set varied in the range 98–160. After addition of 2000 to all step intensities the Rietveld refinement of the structure was repeated. The R-factors from the original and simulated data are listed in Table V.

Only one of the nitrate oxygen atoms, O(6), that in both refinements suffered from significant coordinate shifts showed deviations between the final positions by more than one estimated standard deviation. There were no appreciable differences between the estimated standard deviations of the coordinates in the two refinements. The small differences between the Bragg and the structure factor R-values may be explained by the fact that the weights in the simulated data set became more equal. The large differences between the remaining factors in the table illustrate clearly why these factors are only of internal interest for a refinement. This is obvious from the fact that the simulated lower quality data set shows much smaller profile and weighted profile R-factors than the original data set. Thus it is not the value of the minimum reached in the weighted profile R-factor but the structure parameter set obtained from the minimum that is of importance.

Discussion

The crystal structure of $Zn(OH)(NO_3) \cdot H_2O$ is built up from infinite double chains of edge-sharing octahedra $Zn(OH)_{3/3}(NO_3)_1(H_2O)_{2/2}$ parallel to [010], as shown by the stereoscopic view in Fig. 3. The sixfold coordination of Zn atoms arises from three hydroxyl ions, two water molecules, and one oxygen atom belonging to a nitrate group (see Table IV). The distances from the two water molecules to the O(3) and O(6) atoms of the nitrate groups are consistent with the criteria valid for hydro-

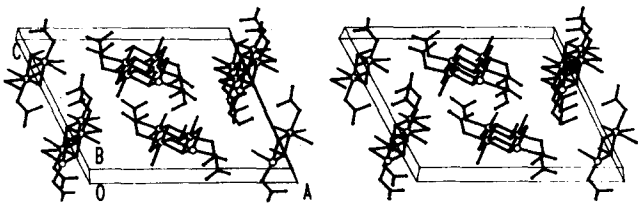

FIG. 3. Stereoscopic view of $Zn(OH)(NO_3) \cdot H_2O$.

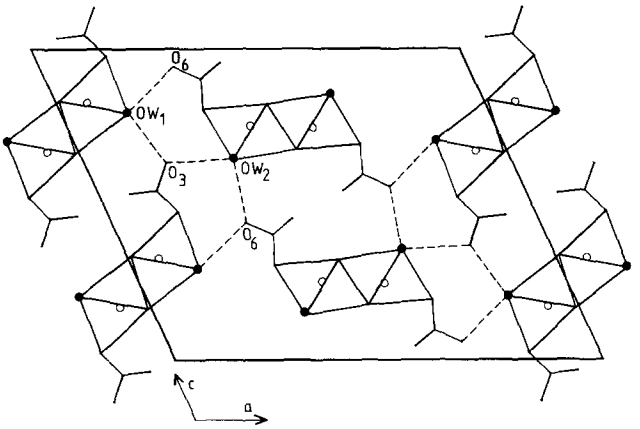

FIG. 4. Projection of the structure of $Zn(OH)(NO_3) \cdot H_2O$ along [010].

gen bonds (*19*). Therefore, the chains are linked together by hydrogen bonds from water molecules to the terminal nitrate groups in neighboring chains. Figure 4 shows the structure projected along the fiber axis, with the hydrogen bonds indicated by dotted lines. Two distinct orientations of the double chains exist in the plane perpendicular to the *b*-axis (the angle between the two orientations is approximately 50°). The corners shared by three octahedra in a chain are occupied by hydroxyl ions; all corners shared by only two octahedra are occupied by water molecules, and the terminal unshared corners are occupied by nitrate oxygen atoms (Fig. 5). This structure

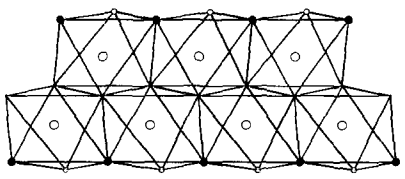

FIG. 5. Double chain of the $Zn(OH)_{3/3}(NO_3)_1(H_2O)_{2/2}$ octahedra. Zn (large circles), H_2O (solid circles), and NO_3 (small circles). (For clarity, the complete NO_3 groups, approximately perpendicular to the chain, are omitted.

model satisfactorily explains the fibrous character of the crystals. It does not belong to the structural classification proposed for zinc hydroxide nitrates (*3*). However, it is interesting to note that these MX_3 double chains suggest new approaches to the interpretation of the transformation of $Zn(OH)(NO_3) \cdot H_2O$ into $Zn_3(OH)_4(NO_3)_2$ by thermal decomposition. As described previously (*8*), calorimetric measurements have shown that gaseous HNO_3 and H_2O are formed during the decomposition reaction

$$3Zn(OH)(NO_3)H_2O \xrightarrow{60\text{–}110°C} Zn_3(OH)_4(NO_3)_2 + HNO_3 + 2H_2O.$$

The zinc hydroxide nitrate $Zn_3(OH)_4(NO_3)_2$ has a layer structure derived from the brucite type, in which some OH^- ions are replaced by O atoms of NO_3 groups (monoclinic structure with $a = 7.038$ Å, $b = 9.658$ Å, $c = 11.182$ Å, and $\beta = 100.96°$). An examination of Fig. 4 shows that some general features of the $Zn(OH)(NO_3) \cdot H_2O$ structure (a set of parallel double chains, whose interchain distance is imposed by the nitrate groups) have a striking similarity with the $Zn_3(OH)_4(NO_3)_2$ layer structure. In order to support this observation, the de-

composition of a fibrous crystal of $Zn(OH)(NO_3) \cdot H_2O$ was studied by means of a single-crystal rotation technique. The *b*-axis was adjusted to be perpendicular to the X-ray beam (Cu$K\alpha$). The decomposition of the crystal of $Zn(OH)(NO_3) \cdot H_2O$ was induced by slow heating to 120°C of the oriented crystal on its goniometer support without changing its orientation. The photograph obtained from this pseudomorph showed the oriented structural character of the transformation, with the relation

$$[010]Zn(OH)(NO_3) \cdot H_2O \;//\; [010]Zn_3(OH)_4(NO_3)_2.$$

During the transformation, the infinite MX_3 double chains lose, per three formula units, two molecules of water, one HNO_3 molecule formed by a nitrate group, and a proton from a water molecule located in an adjoining chain. At this stage of the analysis the OH^- ions remain unchanged. This leaves a hypothetical incomplete structure with empty sites on each side of the chains. The formation of the $Zn_4(OH)_3(NO_3)_2$ layer structure can then be explained by a rotation of 50° of one family of proposed incomplete chains into a suitable orientation, and then a condensation of them in order to fill the active empty sites. In the systematic classification scheme of topotactic reactions proposed by Günter and Oswald (*20*), the chemical reaction given above is characterized by the conservation of one-dimensional structural elements during the transformation.

Final Remarks

To conclude, despite the fibrous character of the crystals of the zinc hydroxide nitrate $Zn(OH)(NO_3) \cdot H_2O$, its crystal structure has been solved and refined by combining single-crystal and powder diffraction techniques. The application of the Rietveld method to powder data has fully revealed the details of the structure. This example, in which the crystals exhibit specific textural properties, illustrates the power of the Rietveld refinement procedure for complete structure analysis. From the chemical point of view, the structure solution described in this paper contributes to a better understanding of the physicochemical properties of the zinc hydroxide nitrates, as shown by the proposed interpretation of the topotactic transformation of $Zn(OH)(NO_3) \cdot H_2O$ into $Zn_3(OH)_4(NO_3)_2$. Moreover, the Rietveld refinements of several sets of powder diffraction data, obtained under different experimental conditions, and including one set with a high simulated background, have shown that the intercomparison is better made using the structural indicators R_F and R_B. Clearly, the R_p and R_{wp} factors are the meaningful indicators to follow the refinement process with one specific data set.

Acknowledgments

This work has received financial support from the Swedish Natural Science Research Council and the Centre National de la Recherche Scientifique.

References

1. W. Stählin, and H. R. Oswald, *Acta Crystallogr. B* **26,** 860 (1970).
2. M. Louër, D. Grandjean, and D. Weigel, *Acta Crystallogr. B* **29,** 1703 (1973).
3. M. Louër, D. Louër, and D. Grandjean, *Acta Crystallogr. B* **29,** 1696 (1973).
4. W. Stählin and H. R. Oswald, *J. Solid State Chem.* **3,** 256 (1971).
5. D. Louër, *Chem. Scr. A* **26,** 17 (1986).
6. W. Stählin and H. R. Oswald, *J. Solid State Chem.* **2,** 252 (1971).
7. M. Louër, D. Louër, D. Grandjean, and D. Weigel, *Acta Crystallogr. B* **29,** 1707 (1973).
8. J. P. Auffredic and D. Louër, *J. Solid State Chem.* **46,** 245 (1983).
9. P.-E. Werner, *Chem. Scr. A* **26** 57 (1986).
10. H. M. Rietveld, *J. Appl. Crystallogr.* **2,** 65 (1969).

11. D. LOUËR, M. LOUËR AND D. WEIGEL, *C.R. Acad. Sci. Paris* **266,** 59 (1968).
12. K.-E. JOHANSSON, T. PALM, AND P.-E. WERNER, *J. Phys. E* **13,** 1289 (1980).
13. C. R. HUBBARD, H. E. SWANSON, AND F. A. MAUER, *J. Appl. Crystallogr.* **8,** 45 (1975)
14. P.-E. WERNER, S. SALOMÉ, G. MALMROS, AND J. THOMAS, *J. Appl. Crystallogr.* **12,** 107 (1979)
15. H. TORAYA, *J. Appl. Crystallogr.* **18,** 351 (1985).
16. D. B. WILES, A. SAKTHIVEL, AND R. A. YOUNG, Program DBW3.2S (1987).
17. D. B. WILES AND R. A. YOUNG, *J. Appl. Crystallogr.* **14,** 149 (1981).
18. P.-E. WERNER, *Chem. Scr.* **6,** 1 (1981).
19. W. H. BAUR, AND A. A. KHAN, *Acta Crystallogr. B* **26,** 1584 (1970).
20. J. R. GÜNTER AND H. R. OSWALD, *Bull. Inst. Chem. Res. Kyoto Univ.* **53,** 249 (1975)